

Article

Centrifugal Microfluidic Integration of 4-Plex ddPCR Demonstrated by the Quantification of Cancer-Associated Point Mutations

Franziska Schlenker¹, Elena Kipf¹, Nadine Borst^{1,2}, Nils Paust^{1,2}, Roland Zengerle^{1,2}, Felix von Stetten^{1,2}, Peter Juelg^{1,†}  and Tobias Hutzenlaub^{1,2,*,†}

- ¹ Hahn-Schickard, Georges-Koehler-Allee 103, 79110 Freiburg, Germany; Franziska.schlenker@hahn-schickard.de (F.S.); elena.kipf@hahn-schickard.de (E.K.); Nadine.Borst@Hahn-Schickard.de (N.B.); Nils.Paust@hahn-schickard.de (N.P.); Roland.Zengerle@Hahn-Schickard.de (R.Z.); Felix.von.Stetten@Hahn-Schickard.de (F.v.S.); Peter.Juelg@Hahn-Schickard.de (P.J.)
- ² Laboratory for MEMS Applications, IMTEK—Department of Microsystems Engineering, University of Freiburg, Georges-Koehler-Allee 103, 79110 Freiburg, Germany
- * Correspondence: Tobias.Hutzenlaub@Hahn-Schickard.de; Tel.: +49-761-203-73269
- † Contributed equally.

Abstract: We present the centrifugal microfluidic implementation of a four-plex digital droplet polymerase chain reaction (ddPCR). The platform features 12 identical ddPCR units on a LabDisk cartridge, each capable of generating droplets with a diameter of $82.7 \pm 9 \mu\text{m}$. By investigating different oil–surfactant concentrations, we identified a robust process for droplet generation and stabilization. We observed high droplet stability during thermocycling and endpoint fluorescence imaging, as is required for ddPCRs. Furthermore, we introduce an automated process for four-color fluorescence imaging using a commercial cell analysis microscope, including a customized software pipeline for ddPCR image evaluation. The applicability of ddPCRs is demonstrated by the quantification of three cancer-associated *KRAS* point mutations (G12D, G12V and G12A) in a diagnostically relevant wild type DNA background. The four-plex assay showed high sensitivity (3.5–35 mutant DNA copies in 15,000 wild type DNA copies) and linear performance ($R^2 = 0.99$) across all targets in the LabDisk.

Keywords: microfluidics; digital droplet polymerase chain reaction (ddPCR); multiplexing; centrifugal step emulsification; droplet stability; droplet fluorescence evaluation



Citation: Schlenker, F.; Kipf, E.; Borst, N.; Paust, N.; Zengerle, R.; von Stetten, F.; Juelg, P.; Hutzenlaub, T. Centrifugal Microfluidic Integration of 4-Plex ddPCR Demonstrated by the Quantification of Cancer-Associated Point Mutations. *Processes* **2021**, *9*, 97. <https://doi.org/10.3390/pr9010097>

Received: 30 November 2020

Accepted: 23 December 2020

Published: 5 January 2021

Publisher's Note: MDPI stays neutral with regard to jurisdictional claims in published maps and institutional affiliations.



Copyright: © 2021 by the authors. Licensee MDPI, Basel, Switzerland. This article is an open access article distributed under the terms and conditions of the Creative Commons Attribution (CC BY) license (<https://creativecommons.org/licenses/by/4.0/>).

1. Introduction

Digital polymerase chain reaction (dPCR) allows the precise and absolute quantification of nucleic acids without the need for standard curves [1,2]. Due to its sensitivity, dPCR is particularly useful for detecting low target concentrations in complex backgrounds, such as rare point mutations in a background of non-mutated wild type DNA [3]. In contrast to conventional quantitative PCR, the reaction mix is partitioned into thousands of compartments using either pre-defined stationary cavities or aqueous droplets in oil [4–7]. In recent years, the latter approach, digital droplet PCR (ddPCR), has become the most common, with companies such as Bio-Rad and Stilla Technologies releasing commercial systems [8]. One of the key factors for a successful ddPCR is the ability to generate emulsions that are stable throughout the complete analytic workflow. This is especially challenging during DNA amplification, when temperature cycling induces thermal stress [9]. The most basic approach is to stabilize these emulsions with surfactants in the oil phase. However, this is typically not sufficient, and further measures of droplet stabilization have been introduced. Bio-Rad additionally uses reagents which encapsulate the droplets with a protein skin by applying heat. However, this has the downside that the customer is limited to a specific

PCR mix, obtained from Bio-Rad [10,11]. Stilla Technologies generates and cycles the droplets in their device by applying up to 950 mbar of overpressure to stabilize them. This requires an external pressure source that is not available in all settings (e.g., at the point of care (PoC)) [12].

In this work, we investigate the influence of surfactant concentration and oil combinations for a ddPCR without any additional means of stabilization. Furthermore, we introduce a simple and robust laboratory workflow for image analysis of a four-color ddPCR performed inside a microfluidic cyclo-olefin copolymer (COC) cartridge. Our work is based on centrifugal microfluidic step emulsification, as introduced by Schuler et al. [9]. In the recent past, centrifugal microfluidics developed into a mature technology which enabled the efficient miniaturization, parallelization and integration of assays for both sample preparation and analysis [13–15]. In the past, several groups have presented centrifugal, microfluidic cartridges that were able to emulsify a reaction mix [6,9,16–20]. We present a centrifugal, microfluidic, single-use cartridge (LabDisk) with 12 identical ddPCR units. In contrast to the state of the art, where until now only one-plex ddPCR assays have been automated by centrifugal microfluidics [9,17–19], we present an increased multiplexing degree of four. This elevated degree of multiplexing is particularly relevant for cancer diagnostics, where a comprehensive overview of the mutation status of a patient must be generated from a limited sample amount [3]. We demonstrate this high degree of multiplexing for point mutations in colorectal carcinoma. In one reaction, we quantify three *KRAS* mutations (G12D, G12V and G12A) in a background of their corresponding wild type sequence. By simultaneously quantifying the wild type, one can determine diagnostically relevant mutant to wild type allele frequencies. In proof-of-concept experiments with serial dilutions of a DNA template, we investigate the assay linearity and sensitivity for all targets.

2. Materials and Methods

2.1. LabDisk Design and Manufacturing

The computer-aided design layout of the ddPCR unit (see Figure 1A) and the final LabDisk with 12 of these ddPCR units were designed using Solidworks (Dassault Systèmes). Each ddPCR unit included an inlet to transfer the reagents into the reaction chamber. A supply channel (width of 40 μm and depth of 40 μm) connected the inlet and the reaction chamber. The distance between the sealing foil and the bottom of the chamber was defined by a pyramidal structure [9] with a minimum depth of 80 μm and a maximum depth of 160 μm . The supporting structures (pillars) with a diameter of 500 μm ensured this distance. As indicated in Figure 1A, four identical nozzles, each with a width of 24 μm and a depth of 15 μm , were used for parallel droplet generation. The ddPCR unit was vented by a hole on the far side of the LabDisk.

The Hahn-Schickard foundry service manufactured the LabDisks. The fabrication of the master tool started with precision milling of polymethyl methacrylate (PMMA), followed by soft lithography to create the flexible polydimethylsiloxane (PDMS) master. The manufacturing process included the micro-thermoforming and thermal sealing of the cartridges [21]. The 300 μm COC foils (COC8007/COC6013) from Tekniple were thermoformed using the PDMS master tool. These structured foils were thermally sealed by 200 μm foil (COC8007/COC6013, Tekniple). Polytetrafluoroethylene (PTFE) membranes (PMV15N, POREX [22]) on the far side of the LabDisk closed the venting holes to prevent evaporation during thermocycling. After reagent transfer, the inlet holes were closed by a pressure-sensitive adhesive foil (9795R from 3M). To improve the distribution of hot air, a 1 mm thick cover (PMMA, Evonik) with cutouts between each ddPCR unit was put on top of the disk before thermocycling (Figure S5, see electronic supplementary information (ESI)).

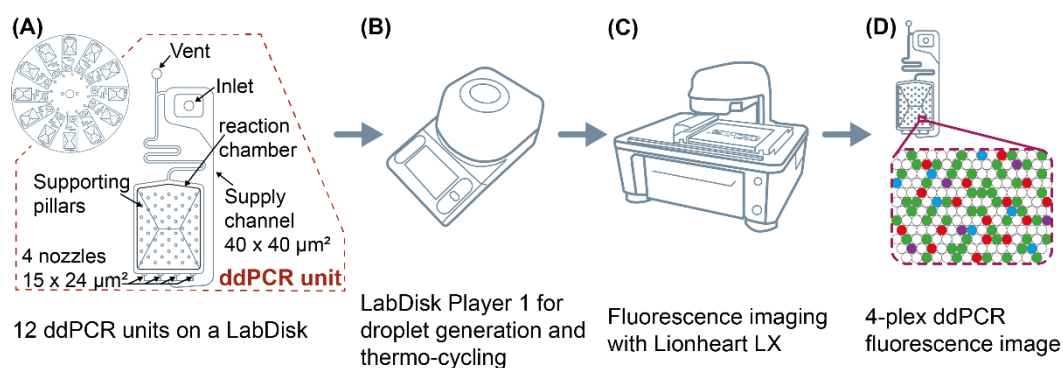


Figure 1. Workflow for an automated four-plex digital droplet polymerase chain reaction (ddPCR) in a LabDisk. (A) LabDisk with 12 identical ddPCR units. Each unit consisted of an inlet, a venting structure, a supply channel, a reaction chamber with supporting pillars and four nozzles for droplet generation by centrifugal step emulsification. (B) Droplet generation and thermocycling in LabDisk Player 1. (C) Fluorescence imaging with an automated Lionheart LX fluorescence microscope. (D) Four-plex ddPCR fluorescence image and data evaluation with Gen5 software to evaluate the assay performance.

2.2. PCR Reagents

For proof of concept, a Mediator Probe PCR was employed [23]. This assay principle is of particular interest for point mutations as well as for multiplexing, as the fluorescence signal generation at the universal reporter oligonucleotide is independent from the target sequence detected by label-free mediator probes [24]. The components of the four-plex mediator probe ddPCR mix were as follows: 1× concentrated PerfeCTa Multi-Plex qPCR ToughMix (Quantabio), 1200 nM primers (biomers.net) and mediator probes (biomers.net) [24], 600 nM universal reporters (biomers.net) [24], HaeIII (NEB) digested human genomic DNA (Roche), and gBlock DNA fragments (131 bp, IDT). The preparation of the oligonucleotides and gBlocks and the DNA digestion were performed according to the manufacturers' manuals (see ESI). The 10 μL reaction mix for each dilution step contained 1 μL of wild type DNA and 1 μL of the mutant DNA target, both with a predefined concentration set by a 1× concentrated TE buffer (Tris-EDTA buffer solution T9285-100ML, Sigma-Aldrich) and nuclease-free water (AM9937, Ambion). In the proof of concept dilution series experiment, the four nominal concentrations of mutant DNA were 3540, 354, 35 and 3.5 copies per reaction for each mutant target, whereas the wild type DNA concentration was fixed at approximately 15,000 copies per reaction.

2.3. Droplet Generation and Thermocycling

To guarantee stable droplets during droplet generation and PCR thermocycling, the surfactant concentration and the oil combination must be chosen carefully. Earlier work [9] has already revealed the need for two different types of oil: (1) the emulsification-oil for homogeneous droplet generation and (2) the PCR-oil for droplet stabilization during PCR. In this work, the surfactant (DR-RE-SU-4G, Fluigent [25]) concentrations in the emulsification-oil (Novec7500, 3M [26]) and in the PCR-oil (FC-40, 3M [27]) were optimized.

Droplet generation and thermo cycling was performed in LabDisk Player 1 (DI-ALUNOX, formerly Qiagen Lake Constance). This PoC player (as illustrated in Figure 1B) is a small benchtop device for centrifugal actuation and temperature control. The complete frequency and temperature protocol for droplet cycling and the ddPCR is depicted in Figure 2. The transfer of the emulsification-oil to the reaction chamber was done at 40 Hz (120 s, 5 Hz/s). After pipetting 10 μL of the reaction mix into the inlet, the droplets (approximately 35,000) were generated by centrifugal step emulsification at 60 Hz for 3 min. It is important to accelerate to 60 Hz rapidly (15 Hz/s) in order to generate the droplets at a constant frequency. After droplet generation, the player was stopped (deceleration of 1 Hz/s), and the PCR-oil was pipetted into the inlet. The PCR-oil was transferred at 30 Hz over 10 min, with a very slow acceleration and deceleration rate of 1 Hz/s to avoid

droplet merging. During droplet generation, the temperature remained constant at 25 °C. The ddPCR began with a hot start at 94 °C for 5 min, followed by 45 cycles between 94 °C (15 s) and 56 °C (60 s) and a 10 min cooling step at 25 °C at the end of the cycling protocol. During ddPCR thermocycling, the rotation frequency remained constant at 1 Hz to keep the droplets in the reaction chamber. After PCR thermocycling, the temperature was kept constant at 25 °C to allow the temperature in the ddPCR unit to reach room temperature. As we observed the post-PCR merging of droplets, most likely caused by electrostatic discharge effects, a standard handling procedure was developed: we recommend electrostatic discharge of the user prior to the transfer of the disk from LabDisk Player 1 to a lint-free tissue sprinkled with an antistatic spray (Screen Clene, Advanced Technology Cleaning). Using this procedure, we did not observe any further post-PCR merging effects.

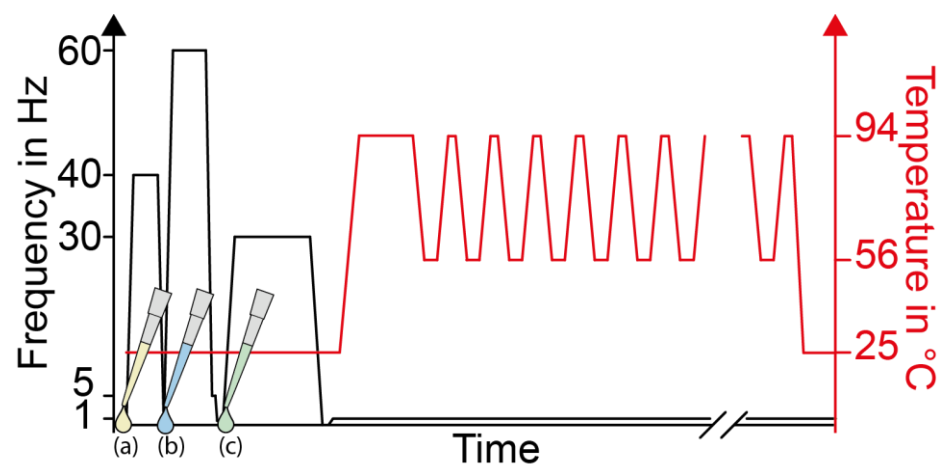


Figure 2. LabDisk frequency and temperature protocol for droplet generation and PCR thermo-cycling in LabDisk Player 1. During droplet generation, the temperature remained constant at room temperature (approximately 25 °C) and the frequency changed, whereas during PCR thermo-cycling, the frequency remained constant at 1 Hz. For oil transfer and droplet generation, the respective reagents were pipetted into the LabDisk manually, as indicated by a pipet tip (emulsification-oil = yellow (a), reaction mix = blue (b) and PCR-oil = green (c)).

2.4. Automated Fluorescence Imaging and Droplet Evaluation

As shown in Figure 1C, the four-plex ddPCR workflow included the fluorescence imaging of each ddPCR unit with a Lionheart LX (Biotek) microscope. For imaging, each ddPCR unit was scanned individually on a British standard microscope slide (ThermoFisher Scientific). Therefore, the LabDisk was cut into 12 parts, each containing a complete ddPCR unit. Each part was attached to a glass slide with adhesive tape. Although it was possible to scan a complete LabDisk with this microscope, scanning time was reduced with this approach. A standard tray (ID 1450527, Biotek) was used to mount the microscope slides with the ddPCR units onto the x/y movable stage of the microscope. Fifty-six individual images were taken of each reaction chamber and in each fluorescence channel with a 2.5 \times -magnification lens. The parameters in the imaging software Gen5 (Biotek) were defined so as to stitch and compress the final image to a size of 50%. The imaging settings for each fluorescence channel are listed in Table 1. The fluorescence channels were defined by a standard fluorophore that could be detected in the respective channel. In this work, the wild type DNA target was detected in the green fluorescent pigment (GFP) channel by a FAM fluorophore, the point mutation for KRAS G12V in the red fluorescent pigment (RFP) channel by a HEX fluorophore, KRAS G12A in the TEXAS RED channel by an AttoRho 101 fluorophore and the KRAS G12D sequence in the Cy5 channel by a Cy5 fluorophore.

Table 1. Settings for imaging with a Lionheart LX microscope.

Channel	Led Intensity	Excitation in MS	Gain	Used Fluorophore in ddPCR	Target
GFP	10	300	24	FAM	Wild type
RFP	10	1000	30	HEX	KRAS G12V
TEXAS RED	10	500	30	AttoRho 101	KRAS G12A
CY5	10	500	30	Cy5	KRAS G12D

The same software as for the imaging process was used for droplet evaluation (Gen5, Biotek). The Gen5 software droplet evaluation pipeline is depicted in the ESI. The intended use of the software and the analysis tool is the counting of cells and cell organelles. However, with small adjustments, this tool can also be used to count droplets and to distinguish between positive and negative droplets. For this purpose, the cellular analysis tool was used to define the background, droplet size and droplet shape (circularity > 0.6), as well as thresholds for the fluorescence intensity measurement. It was important to include circularity as a parameter in the calculation metrics so that dust particles or other artifacts, which did not match the defined droplet shape, could be removed. Further inclusion criteria for a detected droplet were the minimum and maximum object sizes (here, 45 μm and 90 μm). To facilitate the target evaluation, each fluorescence channel was defined as a subpopulation. In this work, there were four different subpopulations, as four channels were used. Each subpopulation needed at least two parameters, the circularity and the mean fluorescence intensity, which should be used to differentiate between positive and negative droplets. The line profile tool provided appropriate thresholds for this purpose. A line was drawn across an area of interest, and the intensity profile of each droplet or structure was shown. A fifth subpopulation counted the droplets with a circularity > 0.6 for the overall droplet count. In this work, the GFP channel had the highest background signal in the droplets, so this signal was used to detect the droplets and determine their total number. As we observed the multi-droplet layers in the outer area of the reaction chamber (Figure S4 in ESI), we limited the evaluation to an inner area where droplet monolayers were guaranteed. On average, 6000 droplets were evaluated for each data point during ddPCR validation. These multi-droplet layers could be reduced by redesigning the reaction chamber and, for example, adjusting the depth to a maximum of 140 μm .

3. Results and Discussion

3.1. LabDisk

The designed LabDisk included 12 identical ddPCR units, as shown in Figure 3A. These units could be used either to test different assay conditions, such as primer and probe concentrations, or to test different assay targets. The LabDisk presented here was a single-use cartridge, which was disposed after each run. The target panel of the proposed LabDisk was not fixed and could easily be adapted for different applications. This is a particular advantage of the employed Mediator Probe PCR assay [24]. A limiting factor might be the application-specific requirements regarding droplet number and droplet size. Figure 3B shows a bright field microscopy image of the generated droplets. Robust droplet generation was achieved with the PerfeCTa MultiPlex qPCR Toughmix.

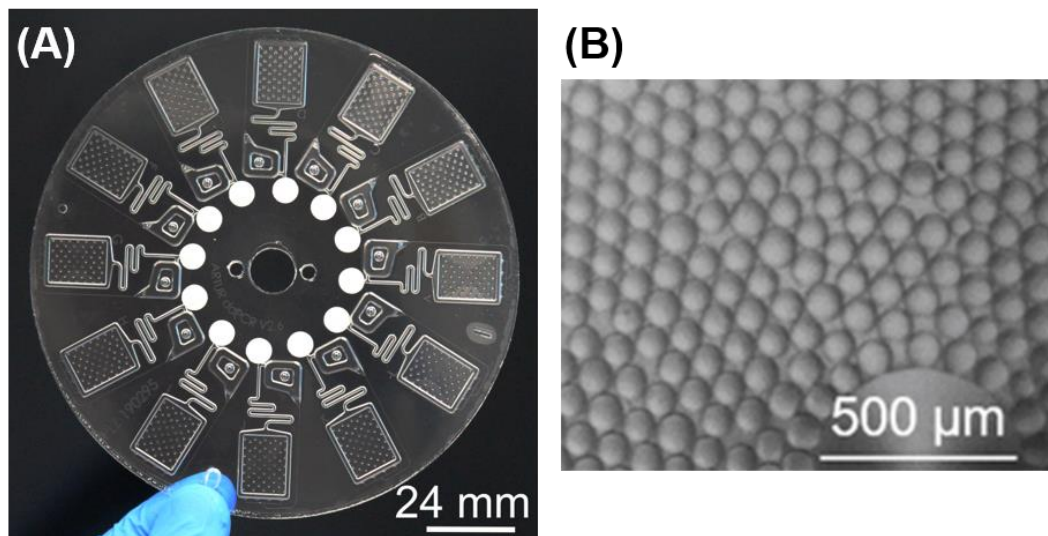


Figure 3. (A) The LabDisk with 12 identical ddPCR units manufactured with cyclo-olefin copolymer (COC) foil technology. On the far side, each vent is closed by a white polytetrafluoroethylene (PTFE) membrane. (B) Bright field microscopy image of droplets generated with PerfeCTa MultiPlex qPCR Toughmix in a ddPCR unit.

3.2. Evaluation of Surfactant Concentrations in the Emulsification Oil and in the PCR Oil

The 12 identical ddPCR units allowed not only a high number of reactions in a diagnostic application but could also be used to efficiently test and optimize different droplet stabilization settings. The recommended surfactant concentration from the supplier (Fluigent) was 2% for droplet generation. We found this given surfactant concentration quite useful for generating homogeneous droplets. However, during PCR cycling, the oil evaporated completely, and substantial droplet merging occurred (Figure 4A). The vapor pressure of the emulsification-oil was 37,627 Pa at 95 °C [26]. Therefore, after droplet generation, a second oil, termed the PCR-oil, was required for the subsequent cycling process. This second oil must have a lower vapor pressure during cycling, so an oil with a vapor pressure of 9503 Pa at 95 °C was chosen as the PCR-oil [27]. The generated droplets were surrounded by the oil phase, and as the evaporation is an effect of the interface to the surrounding air, the evaporation effect of the oils at the interface was significantly stronger than the evaporation of the droplets. For each ddPCR unit, 6 μL of emulsification-oil and 8 μL of PCR-oil were used. Figure 4A shows the combination of the pure PCR-oil (no surfactant) and different surfactant concentrations in the emulsification-oil. As a general outcome, a high surfactant concentration in the emulsification-oil only (i.e., without surfactant in the PCR-oil) did not prevent droplet merging. In this experiment, surfactant concentrations of 2% to 5% in the emulsification-oil were tested. Figure 4A depicts an exemplary image showing a merged droplet area. As the droplets were generated from a PCR mix which included fluorescence probes and target molecules, the merged droplets appeared brighter than the oil and the background of the image. Covering the droplets with the second oil (PCR-oil) had the effect of the reaction chamber remaining filled with oil after PCR cycling. However, the desired droplet stability was still not achieved. This led to the conclusion that the PCR-oil also needed surfactants to stabilize the droplets in the oil phase during cycling, because evaporation means less of the emulsification-oil remains after every cycle. Therefore, 2% surfactant was dissolved in the PCR-oil, and the experiment with different surfactant concentrations in the emulsification-oil (2–10%) was repeated, as shown in Figure 4B. Two combinations showed no merging (4% and 6% surfactant in the emulsification-oil). The exemplary image in Figure 4B shows a reaction chamber with 4% surfactant in the emulsification-oil and 2% surfactant in the PCR-oil. The emulsification-oil (liquid density at 25 °C, 1.61 kg/L) and the PCR-oil (liquid density at 25 °C, 1.86 kg/L) were miscible, which led to the assumption that the final surfactant

concentration in the ddPCR chamber could be averaged. Therefore, it could be worth investigating the surfactant concentration in the emulsification-oil (5–10%) in combination with the pure PCR-oil in further experiments. The resulting surfactant concentration could be strongly dependent on the PCR cycling parameters (temperature and hold times), as the evaporation of the oil is dependent on these parameters. Therefore, the surfactant concentrations in the oil mix should be investigated for each PCR protocol. In this work, the presented combination (4% surfactant in emulsification-oil and 2% surfactant in PCR-oil) was found to be reliable for both droplet generation and droplet stabilization during PCR. A higher surfactant concentration in the emulsification-oil led to slight merging effects, which may have resulted from a partial destabilization of the steric stabilization layer that was generated by the adsorption of surfactant molecules to each droplet [28].

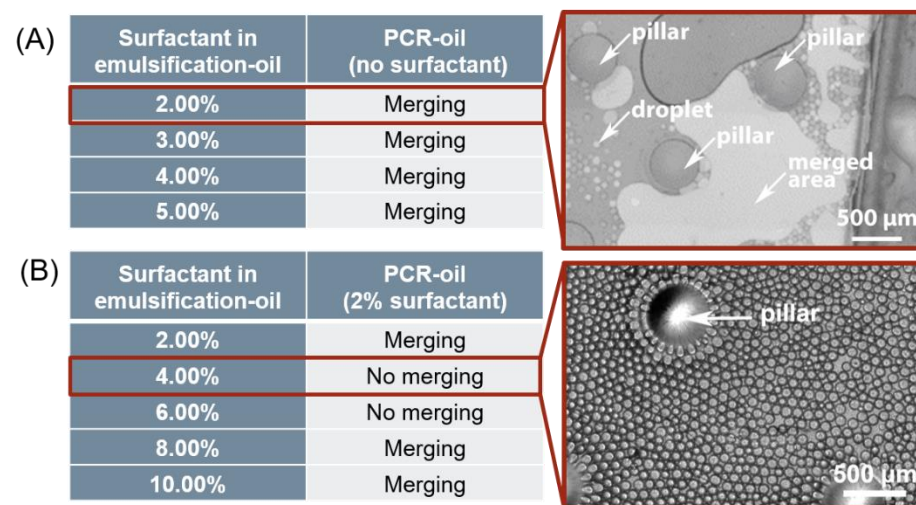


Figure 4. Evaluation of surfactant concentration in emulsification-oil and PCR-oil. (A) A mix of 2–5% surfactant in emulsification-oil combined with pure PCR-oil. The microscopy image shows merged areas as bright. (B) A mix of 2–10% surfactant in emulsification-oil combined with 2% surfactant in PCR-oil. Exemplary microscopy image shows a droplet area with 4% surfactant in emulsification-oil.

3.3. Demonstration of Four-Plex ddPCR in the LabDisk

The data from Figure 4B show two suitable surfactant concentrations (4% and 6% surfactant in emulsification-oil). As the reagent costs increase with the surfactant concentration, the lower concentration was chosen (4% surfactant in the emulsification-oil and 2% surfactant in the PCR-oil). Lower concentrations (e.g., 3% surfactant) might also work, but were not tested. The aim of this experiment was to determine the performance of a four-plex ddPCR assay inside the LabDisk. Figure 5A shows four-color fluorescence images of an assay with a concentration of 3540 DNA copies of each mutant sequence (*KRAS* G12V (blue), G12A (pink) and G12D (red)) in a background of 15,000 wild type DNA copies (green channel). The proof-of-concept experiment with serial dilutions of the DNA template confirmed efficient PCR amplification of each target at concentrations from 3540 mutant copies down to 35 mutant copies (see Figure 5B; full data in ESI). For the mutation sequences *KRAS* G12V and G12A, even the lowest concentrations of 3.5 mutant copies were detectable (limit of detection). At this low concentration, subsampling errors and the quantification of up to 6000 droplets only, instead of all generated droplets, could be reasons for the missing G12D signal. The discrepancy between the detected copy numbers and the spiked copy numbers per μL could be explained by aliquoting errors and by the fact that assay performance is dependent on the PCR protocol. This could result in sub-optimal annealing temperatures for the different targets, as the annealing temperature was fixed at 56 °C. We observed no contamination of the player or the LabDisk, as shown by negative no-template controls (see ESI). This indicates that the PTFE membrane to close the venting hole was functional. In the future, a mechanically closed chip could additionally reduce any remain-

ing risk of contamination. After imaging and droplet detection, the target concentration (see ESI) was calculated using the Poisson equation [5], and the determination coefficient was calculated using the fitting function in Origin (OriginLab). For the calculation of the target concentration, the droplet diameter has to be evaluated. During droplet detection with the Gen5 software, the diameter of each droplet was measured automatically in the fluorescence image. Compared with a bright field image, the fluorescence image provides much better contour detection, because the droplets appear bright on a dark background. The droplet diameter of $82.7 \pm 9 \mu\text{m}$ (histogram; see ESI) was determined with the Lionheart LX microscope ($n = 6000$ droplets). The $10 \mu\text{L}$ of PCR mix led to a final number of approximately 35,000 droplets for each ddPCR unit, as calculated from a measured droplet size of about $83 \mu\text{m}$. Each mutation assay showed very high reaction linearity ($R^2 = 0.99$) within the determined limit of quantification (LoQ = 35 copies per reaction). This proves the functionality of the four-plex ddPCR in the LabDisk and demonstrates its potential for application in cancer monitoring. The readout of all generated droplets could decrease the subsampling error and thus improve the LoQ.

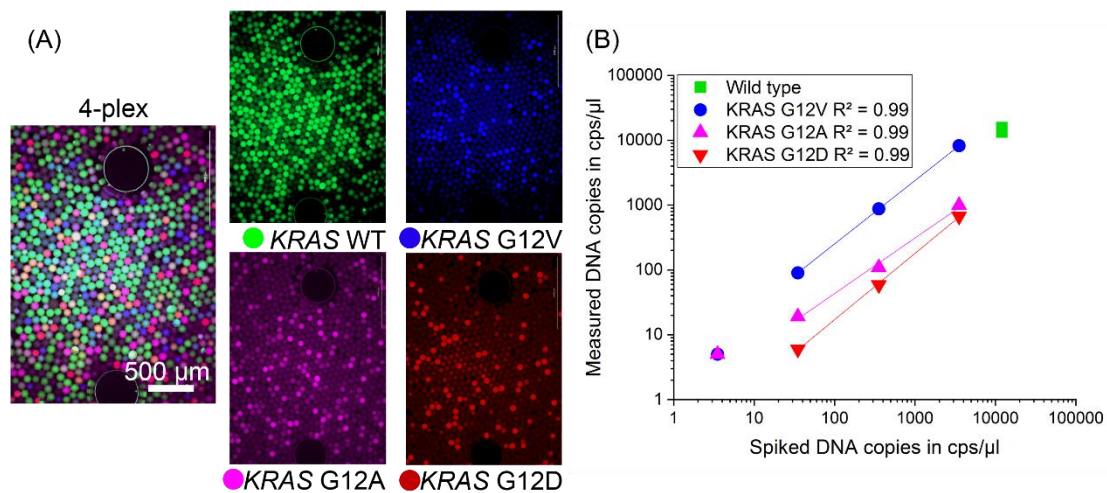


Figure 5. (A) Fluorescence image overlay of the four-plex ddPCR assay for the *KRAS* wild type (WT) and the point mutations *KRAS* G12D, G12V and G12A. Individual fluorescence images show amplification signals in all three color channels for the mutant DNA and in the fourth color channel for the wild type DNA. (B) The proof-of-concept serial dilution experiment showed the high reaction linearity of the four-plex ddPCR assay inside the LabDisk across 3540–35 mutant DNA copies per μL . The lowest dilution point (3.5 mutant DNA copies per μL) was quantifiable for *KRAS* G12V and G12A, but not for G12D.

4. Conclusions and Outlook

This work emphasizes the relevance of surfactant concentrations and oil combinations for achieving stable droplets during droplet generation and PCR thermocycling. Moreover, the presented image evaluation pipeline shows the simplicity of using a commercial fluorescence microscope for droplet counting and four-color ddPCR readout. The introduced four-plex ddPCR workflow on a LabDisk offers great potential for further ddPCR applications. Although shown for cancer targets here, the proposed LabDisk could be used for a broad range of ddPCR applications focusing on the quantification of very low concentrations of point mutations or other DNA sequences in a high wild type DNA background. With these results, we lay the platform for the realization of digital, centrifugal microfluidic sample-to-answer systems for multiplex applications. We think a combination of the presented ddPCR unit with a microfluidic DNA extraction unit on the same cartridge is of particular interest for PoC testing scenarios.

Supplementary Materials: The following are available online at <https://www.mdpi.com/2227-9717/9/1/97/s1>. Preparation of gBlocks. Instruction for HaeIII digestion of human genomic DNA. Supplemental Figure S1: Image evaluation pipeline for droplet counting with Lionheart software Gen5. With the cellular analysis tool, the droplet counting in each ddPCR unit is simplified, as it is an automated process. Important parameters for defining the droplet contour are background values, droplet diameter and droplet shape (circularity). Each fluorescence channel defines a DNA target sequence, and thus it is necessary to adjust the threshold for each channel to determine the positive and negative droplet count. Supplemental Table S1: ddPCR data for four-plex assay. Supplemental Figure S2: images of ddPCR areas after thermocycling. Each picture (A–D) shows a dilution step of synthetic mutant gBlocks in human genomic DNA. Supplemental Figure S3: negative template control of the four-plex ddPCR assay. Image overlay of four-color fluorescence images. Bright artifacts are caused by dust particles on the cartridge surface. Supplemental Figure S4: droplet evaluation in the ddPCR unit. Yellow circles indicate droplets detected by the Gen5 software. The monolayer in the center of the ddPCR area is used for droplet counting. Bright regions in the outer parts of the ddPCR area are due to droplet overlay (multi-droplet layers). Supplemental Figure S5: (A) PMMA cover for thermocycling with cut-outs between each ddPCR unit, and (B) PMMA cover on top of LabDisk to shield ddPCR units from potential temperature overshoots caused by peaks in the dynamically controlled LabDisk Player 1 air heating module's output. Supplemental Figure S6: droplet diameter histogram for the evaluation of 6000 droplets in the green fluorescence channel. The monolayer in the chamber is used for droplet counting and threshold detection.

Author Contributions: Conceptualization, F.S., P.J. and T.H.; methodology, F.S., P.J. and T.H.; Mediator Probe ddPCR assay design and optimization, E.K.; investigation of ddPCR on LabDisk, F.S.; writing—original draft preparation, F.S.; writing—review and editing, all authors; supervision, R.Z., F.v.S., N.P., N.B., P.J. and T.H.; project administration, P.J.; funding acquisition, T.H. All authors have read and agreed to the published version of the manuscript.

Funding: Funding from the Federal Ministry of Education and Research (BMBF), Germany, within the project Artur (grant number 13GW0198F; project management organization VDI Technologiezentrum GmbH), and from the Ministry of Economic Affairs, Labor and Housing of the State of Baden-Württemberg, Germany, within the project PRIMO, is gratefully acknowledged.

Institutional Review Board Statement: Not applicable.

Informed Consent Statement: Not applicable.

Data Availability Statement: Not applicable.

Acknowledgments: We thank the team of the Hahn-Schickard foundry service for the fabrication of the LabDisks. In addition, we want to thank the team of the liquid biopsy lab and the core facility at the University Hospital Freiburg, especially Ulrike Philipp, Max Deuter, Marie Follo, Saskia Hussung and Nikolas von Bubnoff, for supporting the ddPCR assay design and providing the target sequences.

Conflicts of Interest: The authors declare no conflict of interest. The funders had no role in the design of the study; in the collection, analysis or interpretation of the data; in the writing of the manuscript; or in the decision to publish the results.

References

1. Perkins, G.; Lu, H.; Garlan, F.; Taly, V. Droplet-Based Digital PCR: Application in Cancer Research. *Adv. Clin. Chem.* **2017**, *79*, 43–91. [[CrossRef](#)] [[PubMed](#)]
2. Sreejith, K.R.; Ooi, C.H.; Jin, J.; Dao, D.V.; Nguyen, N.-T. Digital polymerase chain reaction technology—Recent advances and future perspectives. *Lab Chip* **2018**, *18*, 3717–3732. [[CrossRef](#)] [[PubMed](#)]
3. Olmedillas-López, S.; García-Arranz, M.; García-Olmo, D. Current and Emerging Applications of Droplet Digital PCR in Oncology. *Mol. Diagn. Ther.* **2017**, *21*, 493–510. [[CrossRef](#)] [[PubMed](#)]
4. Baker, M. Digital PCR hits its stride. *Nat. Methods* **2012**, *9*, 541–544. [[CrossRef](#)]
5. Basu, A.S. Digital Assays Part I: Partitioning Statistics and Digital PCR. *SLAS Technol.* **2017**, *22*, 369–386. [[CrossRef](#)] [[PubMed](#)]
6. Sundberg, S.O.; Wittwer, C.T.; Gao, C.; Gale, B.K. Spinning disk platform for microfluidic digital polymerase chain reaction. *Anal. Chem.* **2010**, *82*, 1546–1550. [[CrossRef](#)]
7. Li, Z.; Liu, Y.; Wei, Q.; Liu, Y.; Liu, W.; Zhang, X.; Yu, Y. Picoliter Well Array Chip-Based Digital Recombinase Polymerase Amplification for Absolute Quantification of Nucleic Acids. *PLoS ONE* **2016**, *11*, e0153359. [[CrossRef](#)]

8. FORTUNE. Market Research Report. Digital PCR Market Size, Share & Industry Analysis, By Type (Droplet Digital PCR, Chip-based Digital PCR, and Others), By Product (Instruments and Reagents & Consumables), by Indication (Infectious Diseases, Oncology, Genetic Disorders, and Others), by End User (Hospitals & Clinics, Pharmaceutical & Biotechnology Industries, Diagnostic Centers, and Academic & Research Organizations), and Regional Forecast 2019–2026. Digital PCR Market FBI102014. 2020. Available online: <https://www.fortunebusinessinsights.com/digital-pcr-market-102014> (accessed on 9 November 2020).
9. Schuler, F.; Trotter, M.; Geltman, M.; Schwemmer, F.; Wadle, S.; Domínguez-Garrido, E.; López, M.; Cervera-Acedo, C.; Santibáñez, P.; von Stetten, F.; et al. Digital droplet PCR on disk. *Lab Chip* **2016**, *16*, 208–216. [[CrossRef](#)]
10. Hindson, B.J.; Ness, K.D.; Masquelier, D.A.; Belgrader, P.; Heredia, N.J.; Makarewicz, A.J.; Bright, I.J.; Lucero, M.Y.; Hiddessen, A.L.; Legler, T.C.; et al. High-throughput droplet digital PCR system for absolute quantitation of DNA copy number. *Anal. Chem.* **2011**, *83*, 8604–8610. [[CrossRef](#)]
11. Hiddessen, A.L.; Chia, E.R. Stabilized Droplets for Calibration and Testing. U.S. Patent 10,240,187, 26 March 2019.
12. Madic, J.; Zocevic, A.; Senlis, V.; Fradet, E.; Andre, B.; Muller, S.; Dangla, R.; Droniou, M.E. Three-color crystal digital PCR. *Biomol. Detect. Quantif.* **2016**, *10*, 34–46. [[CrossRef](#)]
13. Strohmeier, O.; Keller, M.; Schwemmer, F.; Zehnle, S.; Mark, D.; von Stetten, F.; Zengerle, R.; Paust, N. Centrifugal microfluidic platforms: Advanced unit operations and applications. *Chem. Soc. Rev.* **2015**, *44*, 6187–6229. [[CrossRef](#)] [[PubMed](#)]
14. Burger, R.; Amato, L.; Boisen, A. Detection methods for centrifugal microfluidic platforms. *Biosens. Bioelectron.* **2016**, *76*, 54–67. [[CrossRef](#)] [[PubMed](#)]
15. Geissler, M.; Brassard, D.; Clime, L.; Pilar, A.V.C.; Malic, L.; Daoud, J.; Barrère, V.; Luebbert, C.; Blais, B.W.; Corneau, N.; et al. Centrifugal microfluidic lab-on-a-chip system with automated sample lysis, DNA amplification and microarray hybridization for identification of enterohemorrhagic Escherichia coli culture isolates. *Analyst* **2020**, *145*, 6831–6845. [[CrossRef](#)] [[PubMed](#)]
16. Chen, Z.; Liao, P.; Zhang, F.; Jiang, M.; Zhu, Y.; Huang, Y. Centrifugal micro-channel array droplet generation for highly parallel digital PCR. *Lab Chip* **2017**, *17*, 235–240. [[CrossRef](#)] [[PubMed](#)]
17. Schulz, M.; Probst, S.; Calabrese, S.; Homann, A.R.; Borst, N.; Weiss, M.; von Stetten, F.; Zengerle, R.; Paust, N. Versatile Tool for Droplet Generation in Standard Reaction Tubes by Centrifugal Step Emulsification. *Molecules* **2020**, *25*, 1914. [[CrossRef](#)] [[PubMed](#)]
18. Schulz, M.; Calabrese, S.; Hausladen, F.; Wurm, H.; Drossart, D.; Stock, K.; Sobieraj, A.M.; Eichenseher, F.; Loessner, M.J.; Schmelcher, M.; et al. Point-of-care testing system for digital single cell detection of MRSA directly from nasal swabs. *Lab Chip* **2020**, *20*, 2549–2561. [[CrossRef](#)]
19. Li, X.; Zhang, D.; Ruan, W.; Liu, W.; Yin, K.; Tian, T.; Bi, Y.; Ruan, Q.; Zhao, Y.; Zhu, Z.; et al. Centrifugal-Driven Droplet Generation Method with Minimal Waste for Single-Cell Whole Genome Amplification. *Anal. Chem.* **2019**, *91*, 13611–13619. [[CrossRef](#)]
20. Liao, P.; Jiang, M.; Chen, Z.; Zhang, F.; Sun, Y.; Nie, J.; Du, M.; Wang, J.; Fei, P.; Huang, Y. Lossless and Contamination-Free Digital PCR. *bioRxiv* **2019**, 739243. [[CrossRef](#)]
21. Focke, M.; Stumpf, F.; Faltin, B.; Reith, P.; Bamarni, D.; Wadle, S.; Müller, C.; Reinecke, H.; Schrenzel, J.; Francois, P.; et al. Microstructuring of polymer films for sensitive genotyping by real-time PCR on a centrifugal microfluidic platform. *Lab Chip* **2010**, *10*, 2519–2526. [[CrossRef](#)]
22. POREX. PTFE Protection Vents. PMV15N. 2015. Available online: <https://www.porex.com/wp-content/uploads/2020/01/Porex-Datasheet-Virtek-IP-Rated-Protection-Vents.pdf> (accessed on 20 November 2020).
23. Faltin, B.; Wadle, S.; Roth, G.; Zengerle, R.; Stetten, F. von. Mediator probe PCR: A novel approach for detection of real-time PCR based on label-free primary probes and standardized secondary universal fluorogenic reporters. *Clin. Chem.* **2012**, *58*, 1546–1556. [[CrossRef](#)]
24. Lehnert, M.; Kipf, E.; Schlenker, F.; Borst, N.; Zengerle, R.; Stetten, F. von. Fluorescence signal-to-noise optimisation for real-time PCR using universal reporter oligonucleotides. *Anal. Methods* **2018**, *10*, 3444–3454. [[CrossRef](#)]
25. Fluigent. dSURF Product Data Sheet. Available online: https://www.fluigent.com/wp-content/uploads/2018/10/SCL_OPE_001_A-Data-sheet-dSURF.pdf (accessed on 20 November 2020).
26. 3M. 3M Novec 7500 High-Tech Flüssigkeit. 2014. Available online: <https://multimedia.3m.com/mws/media/1438121O/3m-novec-7500-engineered-fluid-tech-sheet.pdf> (accessed on 20 November 2020).
27. 3M. Fluorinert. Electronic Liquid FC-40. Product Information. 2019. Available online: <https://multimedia.3m.com/mws/media/64888O/3m-fluorinert-electronic-liquid-fc40.pdf> (accessed on 20 November 2020).
28. Pichot, R. Stability and Characterisation of Emulsions in the Presence of Colloidal Particles and Surfactants. Ph.D. Thesis, University of Birmingham, Birmingham, AL, USA, 2012.